Hybrid Model for Prediction of Ionospheric Scintillation

Vadim Gherm and Nikolay Zernov,
Department of Radiophysics
University of St.Petersburg, St.Petersburg, Russia

Hal Strangeways,
School of Electronic and Electrical Engineering
University of Leeds, Leeds, U.K.

Sergei Maurits,
Geophysical Institute
University of Alaska, Fairbanks, USA

A Hybrid model for prediction of field scintillation on transionospheric paths of propagation was developed as the combination of the complex phase method (CPM) and random screen technique. In a recent paper [**1**] by Gherm et al., the model was described in detail. The initially developed propagation model [**2**] was solely based on the CPM, or the generalized Rytov's approximation, which is not capable of describing the case of strong scintillation so that, to overcome this restriction, the CPM was combined with the random screen technique. In the contrast with widely employed effective phase screen (e.g. WBMOD, GISM), the random screen introduced in the present method is a physical screen with log-amplitude and phase fluctuations corresponding to a real field on a plane located below the ionosphere. To generate this random screen the relationships for spatial spectra of the phase and log-amplitude correlation functions, as well as their cross-correlation function, are utilized. They are derived in the framework of the CPM. According to the CPM the complex amplitude of the field which has propagated through the ionosphere is represented as follows:

$$E(\mathbf{r},\omega,t)=E_o(r,\omega)R(\mathbf{r},\omega,t), \tag{1}$$

where E_0 is the undisturbed field, R is the random factor. The random factor R is treated in terms of the complex phase

$$R = e^{\psi}, \quad \psi = \chi + iS . \tag{2}$$

Correlation functions of fluctuations of χ and S and their cross -correlation are calculated in ray-centred variables with the variable s oriented along a curved line of sight (path of propagation) determined by a model of the 3-D background ionosphere. Their spatial spectra are given by the following relationships:

$$B_S(\kappa_n,\kappa_\tau) = \frac{\pi k^2}{2}\int_0^{s_0}\frac{ds}{J(s)\varepsilon_0(s)}B_\varepsilon(s,0,\eta_n,\eta_\tau)\cos^2\left\{\frac{1}{2k}\left[\eta_n^2 D_n(s)+\eta_\tau^2 D_\tau(s)+2\eta_n\eta_\tau D_{n\tau}(s)\right]\right\},$$

$$B_\chi(\kappa_n,\kappa_\tau) = \frac{\pi k^2}{2}\int_0^{s_0}\frac{ds}{J(s)\varepsilon_0(s)}B_\varepsilon(s,0,\eta_n,\eta_\tau)\sin^2\left\{\frac{1}{2k}\left[\eta_n^2 D_n(s)+\eta_\tau^2 D_\tau(s)+2\eta_n\eta_\tau D_{n\tau}(s)\right]\right\}, \tag{3}$$

$$B_{S\chi}(\kappa_n,\kappa_\tau)=\frac{\pi k^2}{4}\int_0^{S_0}\frac{ds}{J(s)\varepsilon_0(s)}B_\varepsilon(s,0,\eta_n,\eta_\tau)\sin\left\{\frac{1}{k}\left[\eta_n^2 D_n(s)+\eta_\tau^2 D_\tau(s)+2\eta_n\eta_\tau D_{n\tau}(s)\right]\right\}$$

In equations (3) function J(s) is the Jacobian of transformation of initial transversal variables into current transversal variables along the reference ray of the ray-centred co-ordinate system. In turn, variances of the field phase and log-amplitude fluctuations are derived from equations (3) by integrating in the transversal wave numbers.

Numerical codes are arranged in the way that, on the first step, calculations are solely performed on the basis of the CPM to predict the level of variance of the log-amplitude (or S_4) fluctuations on the Earth's surface in order to check whether the magnitude of this value is within the range of validity of the CPM. If so, the code produces statistical moments (variances of the log-amplitude and phase fluctuations, S_4, frequency spectra of log-amplitude and phase fluctuations) and generates random time series for log-amplitude and phase variations for weak scintillation.

For the opposite case, when the CPM-predicted S_4 on the Earth's surface are too large for the CPM to be valid, the random screen is generated just below the ionosphere. The random spectrum $\widetilde{E}(0,\boldsymbol{\kappa},t)$ of the field generated on the screen below the ionosphere is then transferred to the level of the Earth's surface employing the following relationship of the theory of a random screen

$$\widetilde{E}(z,\kappa,t)=e^{ikz}\widetilde{E}(0,\kappa,t)\exp\left(-\frac{i\kappa^2 z}{2k}\right). \tag{4}$$

It should be additionally stressed that, according to our estimates, for observation points lying inside the ionospheric layer, fluctuations of the field amplitude at frequencies of the order of 1 GHz and higher always have values which are within the range of validity of the CPM. This is true even in the case of very large relative electron density fluctuations and values of TEC. For smaller relative fluctuations and values of TEC this is also true for lower frequencies. This means that propagation in the ionospheric layer for the frequencies mentioned may always be validly described in the scope of the CPM. In turn, this implies that, at L-band and higher frequencies, the regime of strong scintillation does not normally occur inside the ionospheric layer, but may be formed in the region where the field propagates from the ionosphere down to the Earth's surface. This circumstance permits utilization of the CPM to properly introduce the random screen below the ionosphere.

The propagation scintillation model is being constantly updated. In its latest extension a full 3-D model of fluctuations of the electron density of the ionosphere with a single slope inverse power law spatial spectrum of the following form is employed:

$$B_\varepsilon(\vec{\kappa},s)=C_N^2\left[1-\varepsilon_0(s)\right]^2\sigma_N^2(s)\left(1+\frac{\kappa_{tg}^2}{K_{tg}^2}+\frac{\kappa_{tr1}^2}{K_{tr1}^2}+\frac{\kappa_{tr2}^2}{K_{tr2}^2}\right)^{-p/2}. \tag{5}$$

The latter 3-D model is introduced to account for full 3-D local random inhomogeneities with three different outer scales typical of the polar ionosphere. Additionally, the dependence of the variance of fluctuations of the fractional electron density at the points along the reference ray is also taken into account. In equation (5):

- C_N^2 is normalisation coefficient;
- $\varepsilon_0(s)$ is 3-D distribution of the dielectric permittivity of the background ionosphere along the reference ray;
- $\sigma_N^2(s)$ is the variance of the fractional electron density fluctuations.

This paper presents, in particular, first results of prediction of the scintillation effects for high-latitude propagation, derived on the basis of the technique, where the high-resolution model of the polar ionosphere (UAF EPPIM: Eulerian Polar Parallel Ionosphere Model), developed at the University of Alaska, Fairbanks, was integrated with the propagation scintillation model of the University of St.Petersburg, Russia and the University of Leeds, UK [**1,2**].

The University of Alaska, Fairbanks Eulerian Polar Parallel Ionospheric Model (EPPIM) [**3**] is the first principles three-dimensional time-dependent theoretical model. It solves conservation equations of mass, momentum, and energy balance for electrons, seven ion species, and a few minor neutral components of odd nitrogen family, which are important for ionization balance of the lower ionosphere. Specifications of neutral thermosphere (temperature, composition) as well as neutral winds are derived from MSIS and HWM empirical models respectively. All other necessary polar ionosphere inputs are present in the model either as period-specific data, when available, or, in most cases, are derived from statistical/empirical modules, governed by the major geophysical indices (Ap/Kp, F10.7, and IMF parameters). EPPIM covers the region pole ward of 50 degrees of geomagnetic latitude. This choice minimizes occurrences of horizontal trans-boundary fluxes due to horizontal **E** x **B** drift of the polar ionosphere. The model upper boundary (up to 1000 km) is empirically adjusted flux, the lower (80 km) boundary is the condition of photochemical equilibrium. The regular Eulerian grid and parallel computational organization of the model facilitates its high-resolution and, consequently, gradient-resolving capabilities [**4**].

EPPIM is undergoing statistical validation during its continuous run (http://www.arsc.edu/SpaceWeather) with the real-time remote feed of geophysical inputs from NOAA Space Environment Center and other on-line depositories. Massive (~100,000 measurements/year) comparison with ionosounder network shows that typical daytime relative r.m.s. of the foF2 forecast is in the 10-25% range, depending on latitude, while the nighttime range is 20-40%. The comparison also shows that the model statistical biases are reasonably close to zero. Hence, the r.m.s. values above are characteristic of residual random errors of the model, provided it adopts the forecasting method where a period-specific distribution of geophysical drivers governs statistical inputs for ionospheric simulation in a time-dependent manner.

At the present stage, integration of the propagation model and UAF EPPIM utilizes the databases, computed by the high-resolution EPPIM, as the specification of the polar ionosphere environment required for the propagation scintillation model, based on the complex phase method (CPM) [**2**]. Along with the model of the polar ionosphere, the scintillation index S_4 and the variance of phase fluctuations, which are produced in automatic fashion in real time, are the outputs of this model integration for the regime of weak scintillation.

The output of this integrated code is available on the Internet site of the University of Alaska, Fairbanks at the following address: http://www.arsc.edu/SpaceWeather/s4.html. Below in Fig. 1 (a panel from this site) are shown the trajectories of the satellites of the GPS constellation together with values of S4 measured at Gakona and S_4, values for the same scenarios calculated in the approximation of weak scintillation.

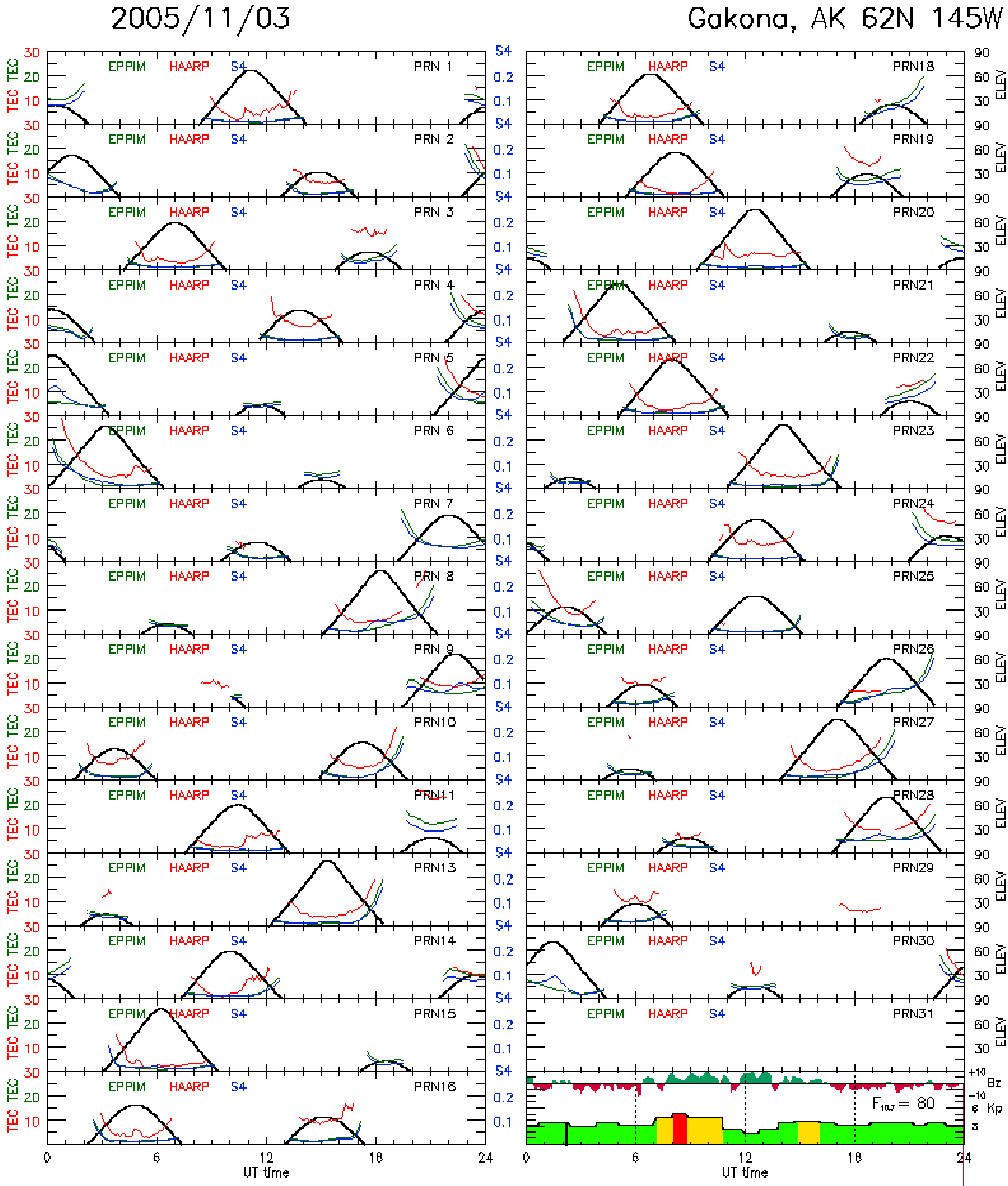

Figure 1. Trajectories of the satellites of the GPS constellation together with values of S_4 measured at Gakona, Alaska and values of S_4, calculated for the same scenarios, in the approximation of weak scintillation.

The plot in Fig. 2 shows the parts of a path of propagation which give the major contribution to the full values of the variances of the field log-amplitude (or S_4) and phase fluctuations. The geophysical conditions and geometry of propagation, for which these results were obtained, will be outlined below. The curves in Fig. 2 clearly show that 90% of the contribution for both the variances of phase and log-amplitude fluctuations are given by the layer of the ionosphere of width 100 km centred on the height of the maximum of the electron density profile of the background ionosphere.

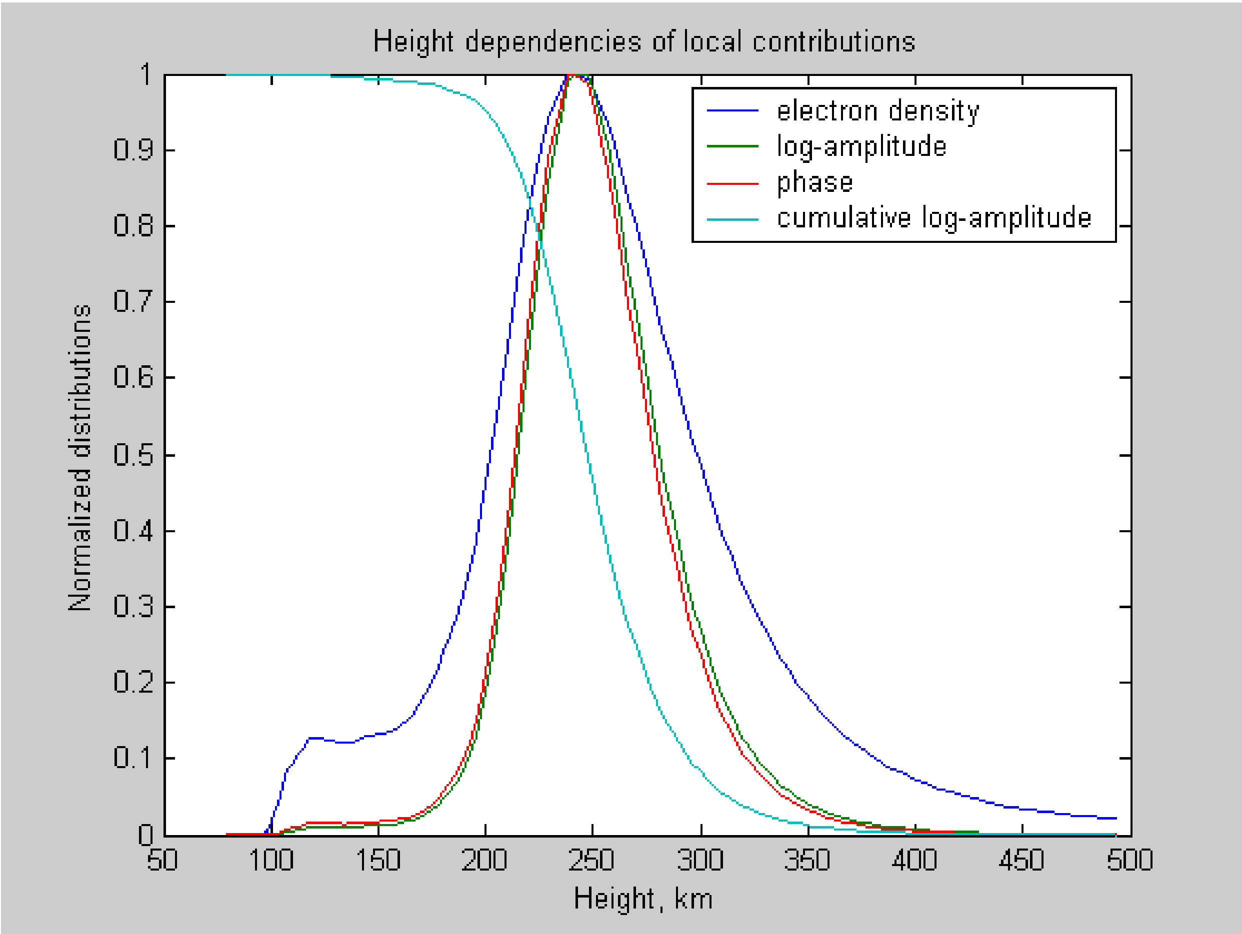

Figure 2. Differential (red- for phase; green- for log-amplitude) and integral (blue) contributions to the variances of the phase and log-amplitude fluctuations. The height electron density profile is given in dark blue.

We also present here the results of prediction of the regime of strong scintillation, which can be produced utilizing EPPIM of the University of Alaska, Fairbanks. It should be pointed out, however, that the order of predicted values of TEC typical for the polar ionosphere does not often meet the conditions for strong scintillation at GPS frequencies. When discussing the factors affecting the level of scintillation, a series of effects should be taken into account. On the one hand, propagation along/close to the Earth's magnetic field lines leads to the enhanced level of the amplitude fluctuations. On the other hand, this type of path of propagation in the polar ionosphere corresponds to almost vertical propagation, and, as has already been stated, vertical TECs are not particularly high in this region. For slant paths of propagation, higher «slant TECs» effectively contribute greater scintillation effects. Then, with sufficiently high values of the fractional electron density, the regime of strong scintillation can be achieved. Additional factors affecting the level of the field scintillation are the spatial shape of random inhomogeneities of the ionosphere and the carrier frequency. The lower the carrier frequency, the higher the level of scintillation.

Two types of «strong scintillation» should be specified:
- ***refractional scintillation***, which is the case when strong phase fluctuations occur together with fairly small amplitude fluctuations. It can be well treated in the scope of the CPM;
- ***diffractional scintillation***, which results in deep fading, so that strong amplitude fluctuations occur together with phase fluctuations. This is the case which is really considered in the theory of wave propagation in random media as the case of strong scintillation, or saturated regime of propagation. The Hybrid method was developed to correctly deal with this.

In a series of figures below results are presented which characterize the effect of scintillation on a GPS-satellite signal at a single observation point for a particular satellite (PRN5) moving in Northern hemisphere. When moving along its trajectory, the elevation angle of the satellite at the receiving location varies from 0 to 75.5^0. The background ionosphere is produced by the EPPIM of the University of Alaska, Fairbanks with a time-step of 5 minutes. Slant 3-D distributions of the electron density along the line of sight from the observation point to a moving satellite are produced with the same time intervals. Random inhomogeneities of the ionosphere are specified by the spatial spectrum of the form (5) with the spectral index of 3.7, the smallest outer scale of 5 km, the cross-magnetic-field aspect ratio of 5, and the longitudinal aspect ratio of 20. Thus, local random ionospheric inhomogeneities are presented as full 3-D shapes, and their parameter values as well as their frozen-in drift velocity (of 500 m/sec), were chosen according to [**5**]. The r.m.s. of the fractional electron density fluctuations at the altitude of the maximum of the electron density of the background ionosphere was taken as 20%.. Calculations were performed for the L-band carrier frequencies of 1600 and 1200 MHz.

In Fig. 3 the r.m.s. of the phase fluctuations and S_4 (upper plot) are presented as functions of time associated with a position along the trajectory of the satellite, and the time dependence of TEC produced by EPPIM is given in the lower plots. In the following series of figures (Figs. 4 to7) statistical characteristics of the field at three particular points of the trajectory and their random time series are given in more detail; viz:
1) the point of the lowest elevation angle of the satellite of 9.25^0
(Figs. 4a,b and Figs. 5a,b);
2) the point of the highest elevation angle of 75.4^0 (Figs. 6a,b);
3) an intermediate point of elevation angle 28.4^0
(Figs. 7a,b).

The case 1) is the situation of very slant propagation. With a chosen value of the fractional electron density r.m.s. of 20%, this demonstrates the situation of strong scintillation with S_4=0.627 and asymmetric probability density function of the intensity fluctuations. Strong scintillation (diffractional scintillation) is even more pronounced for the lower frequency of 1200 MHz, which is characterized by S_4=0.869. For this case the probability density function is even more asymmetric and the shapes of the frequency spectra of the phase and log-amplitude fluctuations differ more from those typical of weak scintillation.

Case 2) is a special case of propagation almost along the line of the Earth's magnetic field leading at ionospheric altitudes leading to an enhanced level of scintillation despite almost vertical propagation with a small vertical TEC. It is characterized by moderate log-amplitude fluctuations (S_4=0.37) with fairly strong phase fluctuations of $\sigma_S = 1.8$ (refractional scintillation).

Finally, the case 3) is a typical case of weak scintillation corresponding to S_4=0.163, with a symmetric probability density function for the intensity fluctuations, and fading frequency spectra of phase and log-amplitude fluctuations with the same high-frequency asymptotic tail.

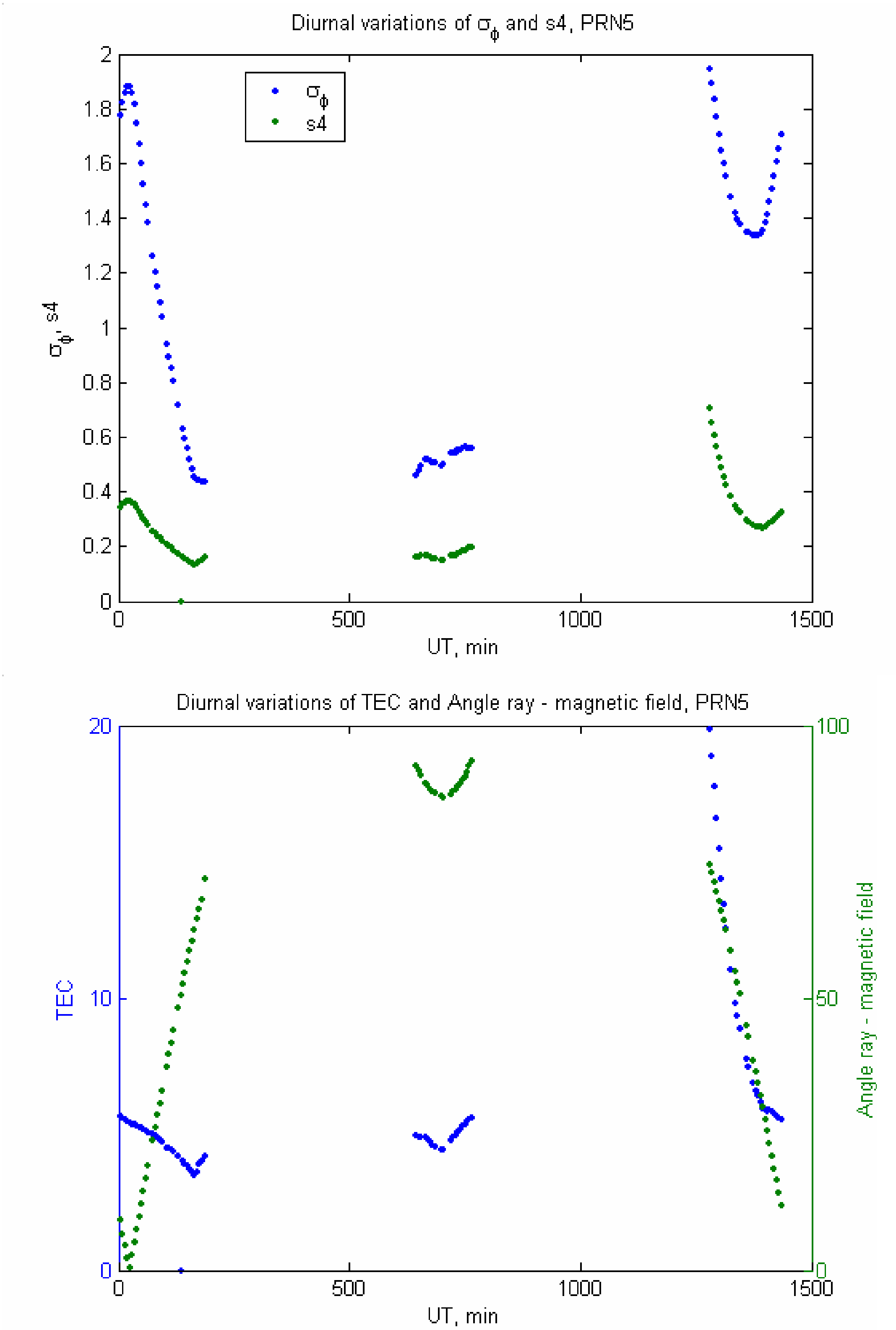

Figure 3. R.m.s. for phase fluctuations and S_4 (upper plot) as functions of time associated with position along the trajectory of the satellite. Time dependence of TEC produced by EPPIM (lower plot).

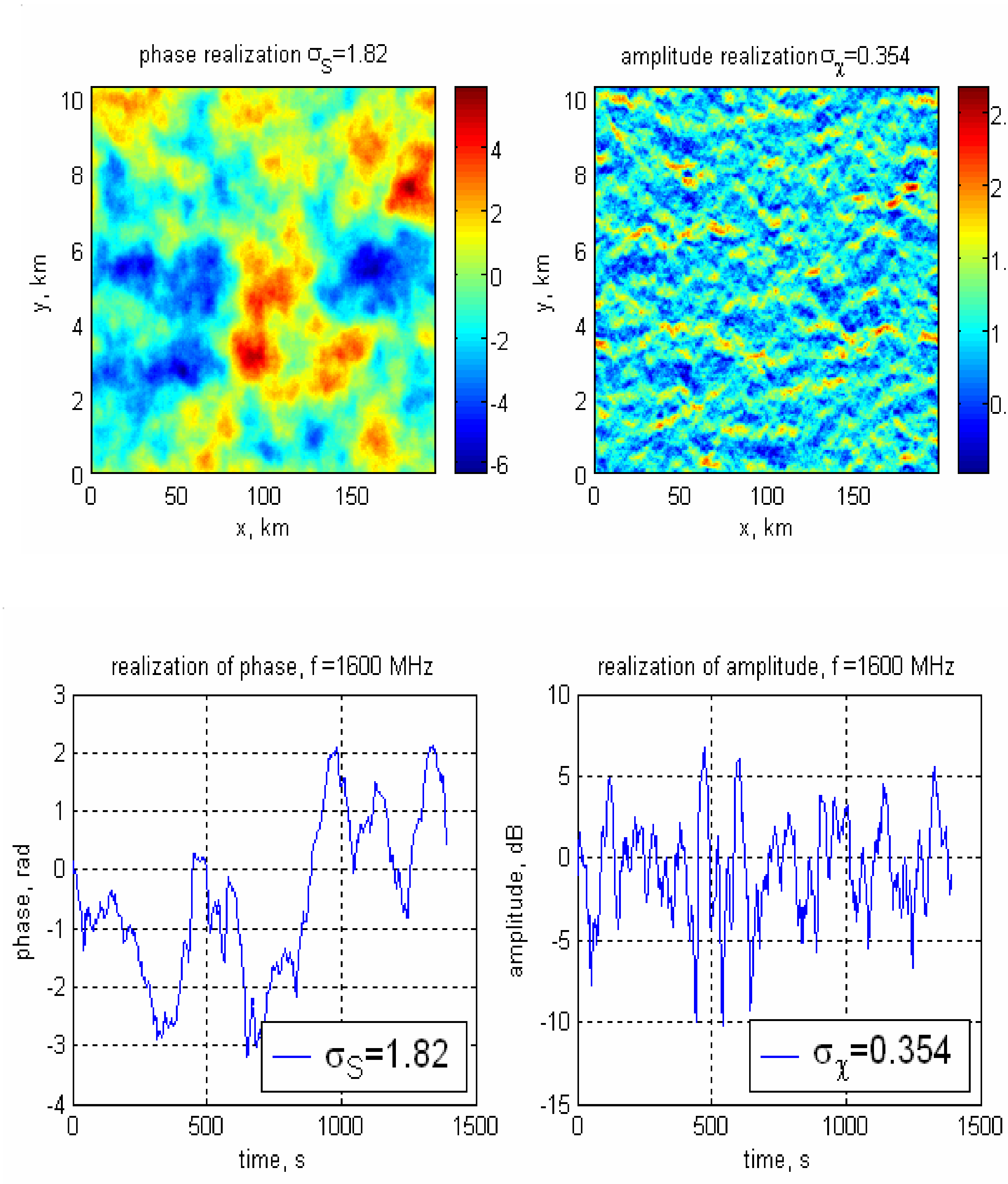

Figure 4a. The case of very slant propagation. Frequency 1600 MHz. Fractional electron density r.m.s. of 20%. Strong scintillation with S_4=0.627. Generated spatial and time realizations on the Earth's surface.

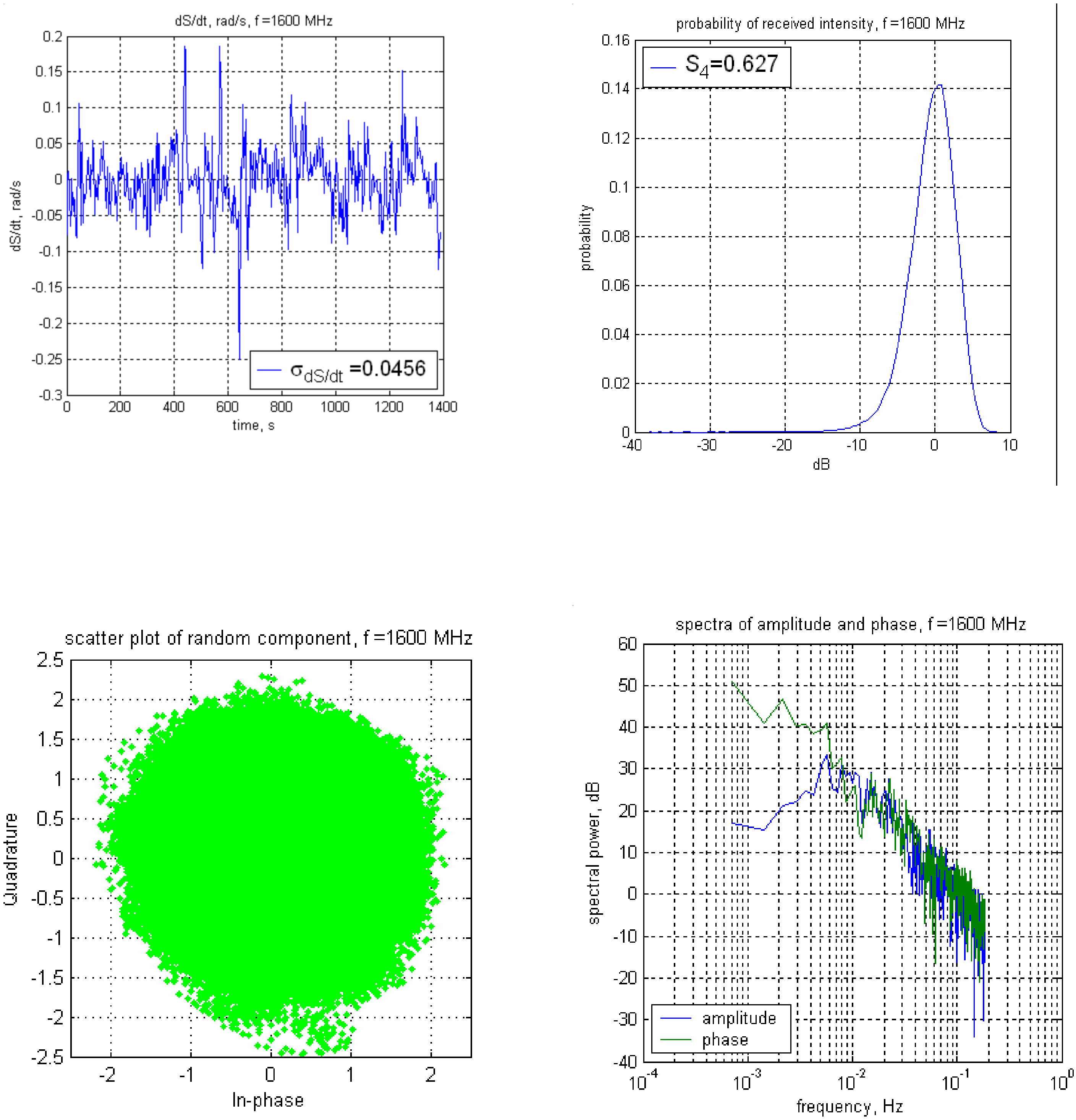

Figure 4b. The case of very slant propagation. Frequency 1600 MHz. Fractional electron density r.m.s. of 20%. Strong scintillation with S_4=0.627 with an asymmetric probability density function of the intensity fluctuations. Also shown are the rate of phase change, the phasor R random walk, and fading frequency spectra of phase and log-amplitude.

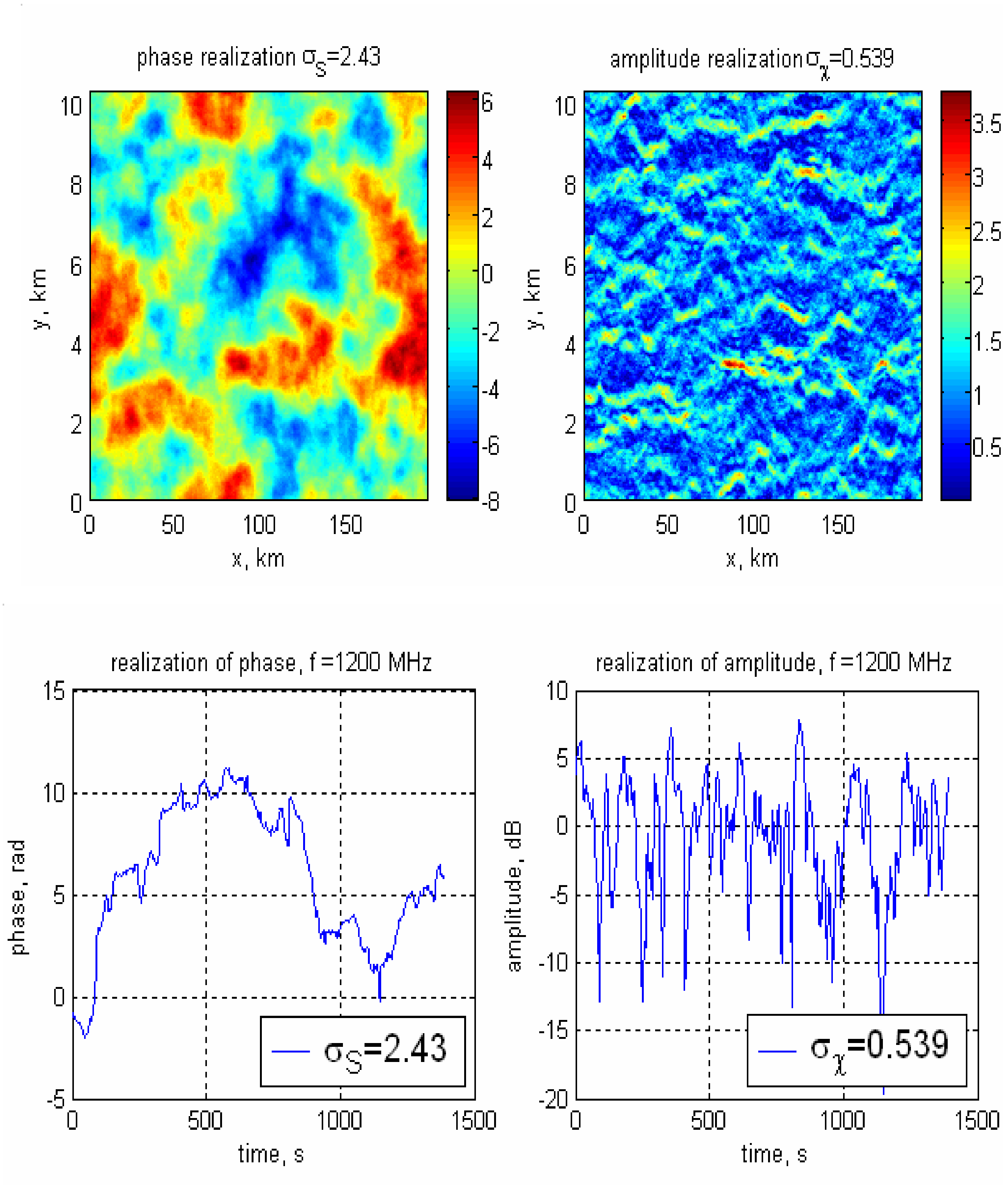

Figure 5a. The case of very slant propagation. Frequency 1200 MHz. Fractional electron density r.m.s. of 20%. Very strong scintillation with S_4=0.869. Generated spatial and time realizations on the Earth's surface.

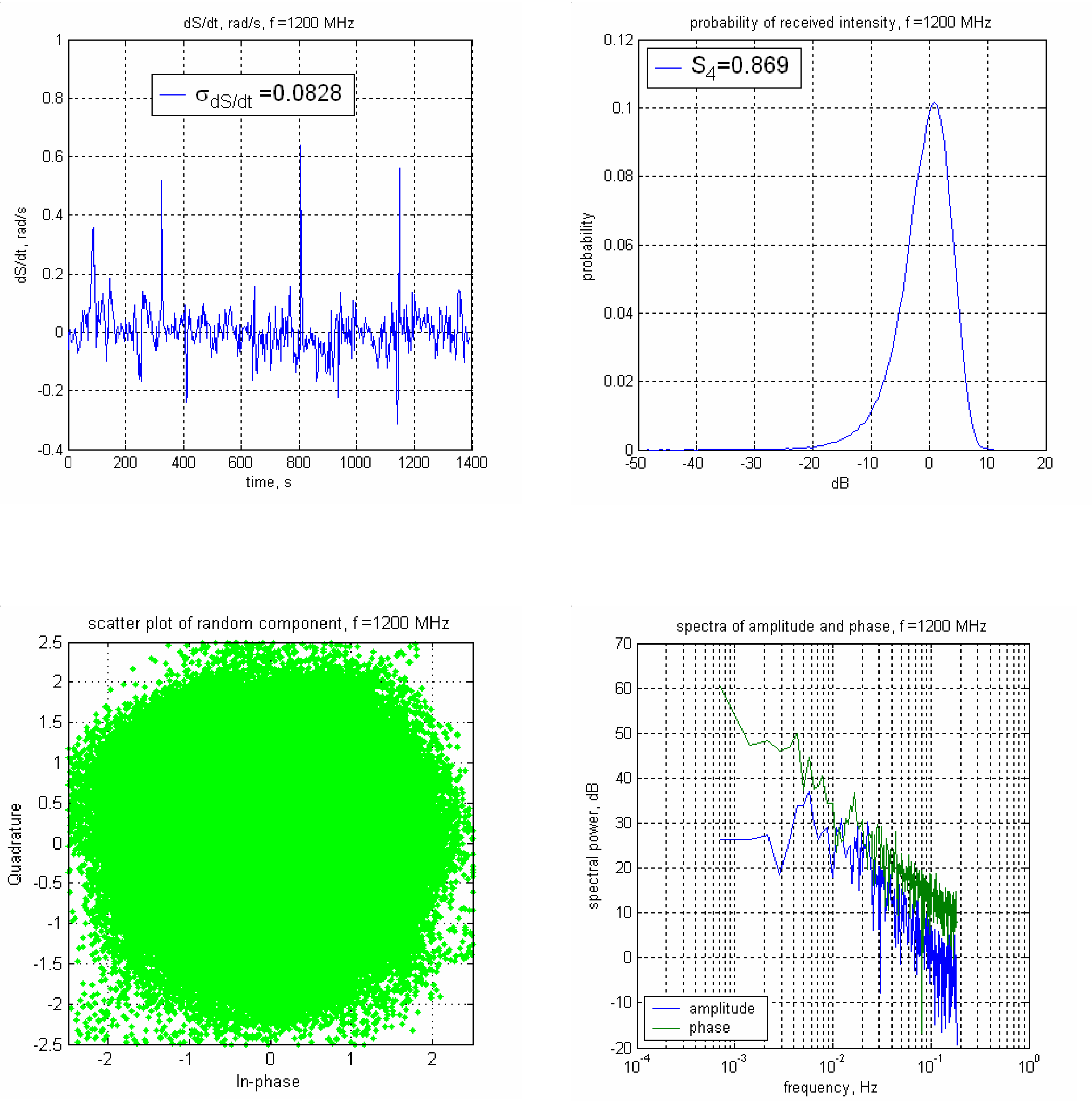

Figure 5b. The case of very slant propagation. Frequency 1200 MHz. Fractional electron density r.m.s. of 20%. Very strong scintillation with S_4=0.869 with a fairly asymmetric probability density function of the intensity fluctuations. Also shown are the rate of phase change, phasor R random walk, and fading frequency spectra of phase and log-amplitude.

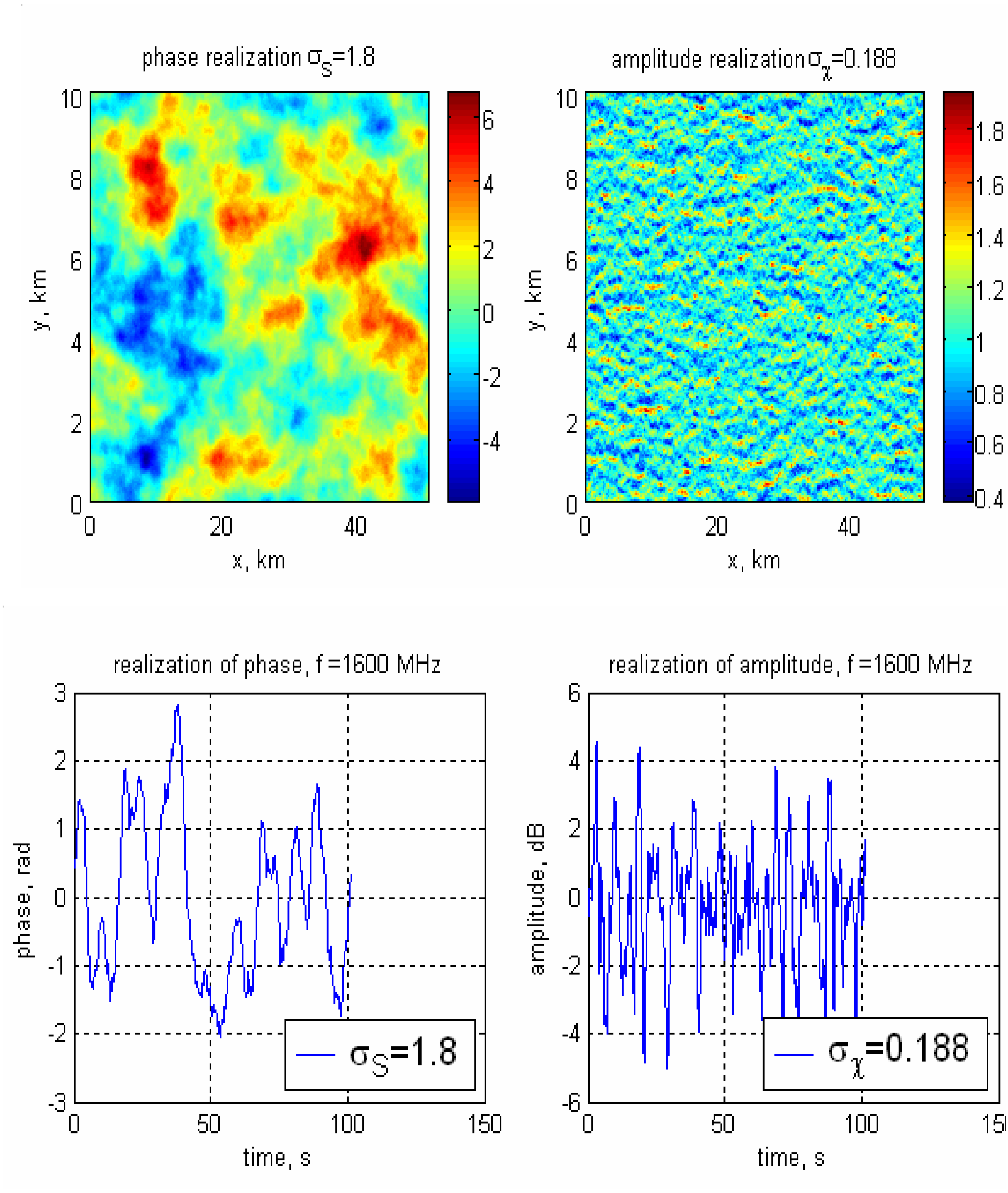

Figure 6a. Propagation along the magnetic field lines. Frequency 1600 MHz. Fractional electron density r.m.s. of 20%. Strong refractional scintillation with fairly high value $\sigma_S = 1.8$ and moderate value of S_4=0.37. Generated spatial and time realizations on the Earth's surface.

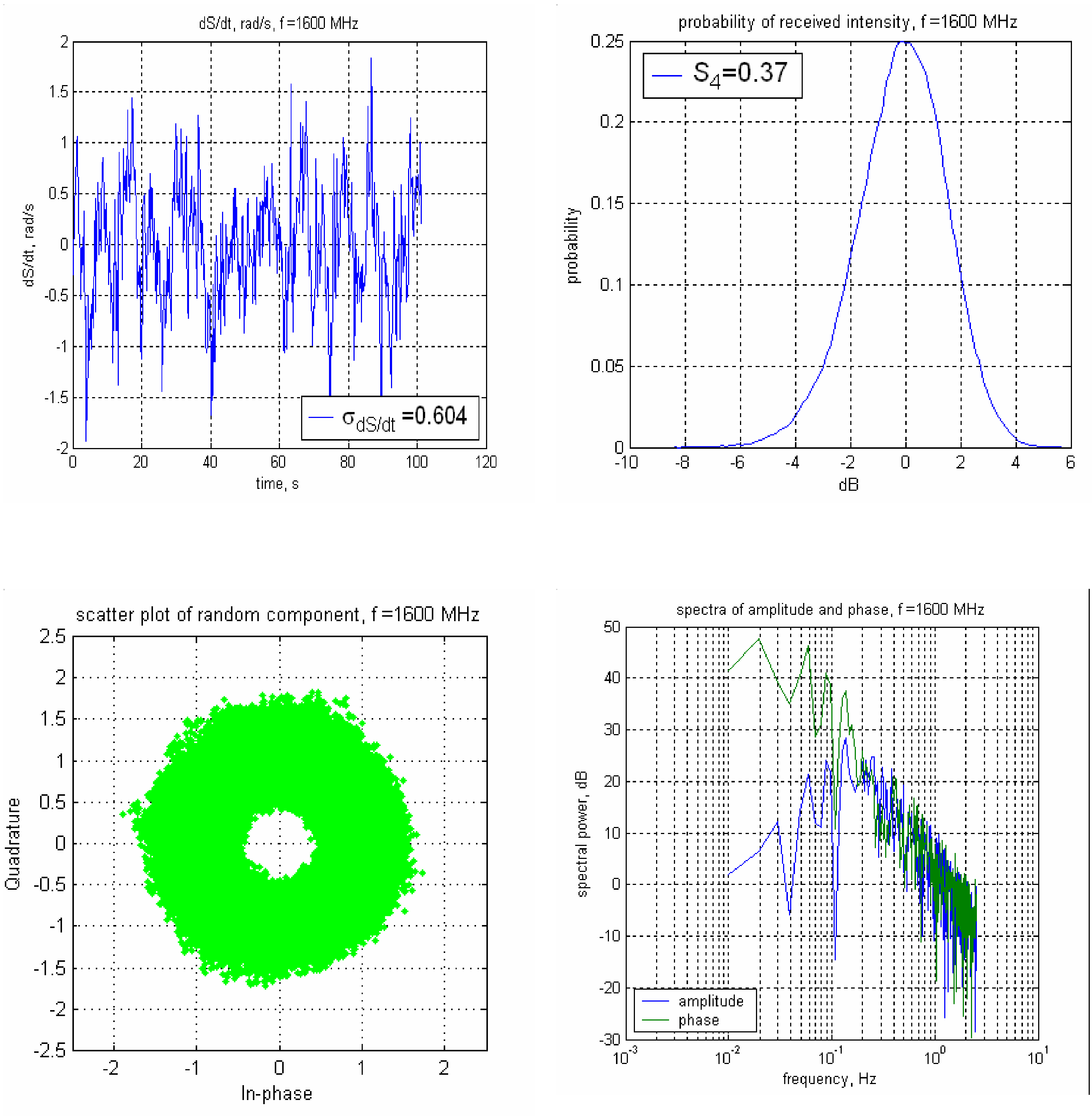

Figure 6b. Propagation along the magnetic field lines. Frequency 1600 MHz. Fractional electron density r.m.s. of 20%. Strong refractional scintillation with fairly high value $\sigma_S = 1.8$ and moderate value of S_4=0.37. Also shown are the rate of phase change, the phasor R random walk, and the fading frequency spectra of phase and log-amplitude.

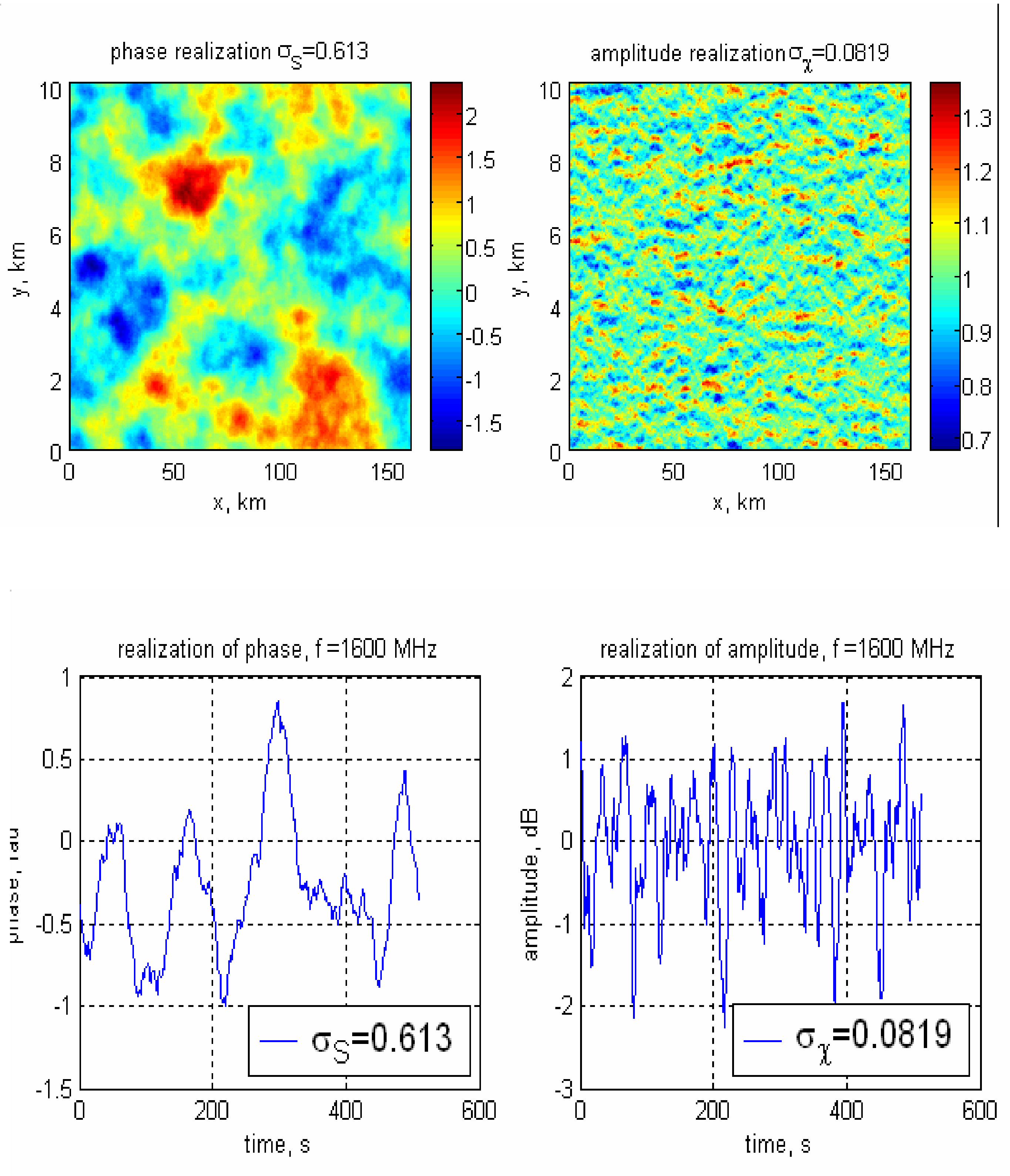

Figure 7a. The intermediate case. Frequency 1600 MHz. Fractional electron density r.m.s. of 20%. Weak scintillation with S_4=0.163. Generated spatial and time realizations on the Earth's surface.

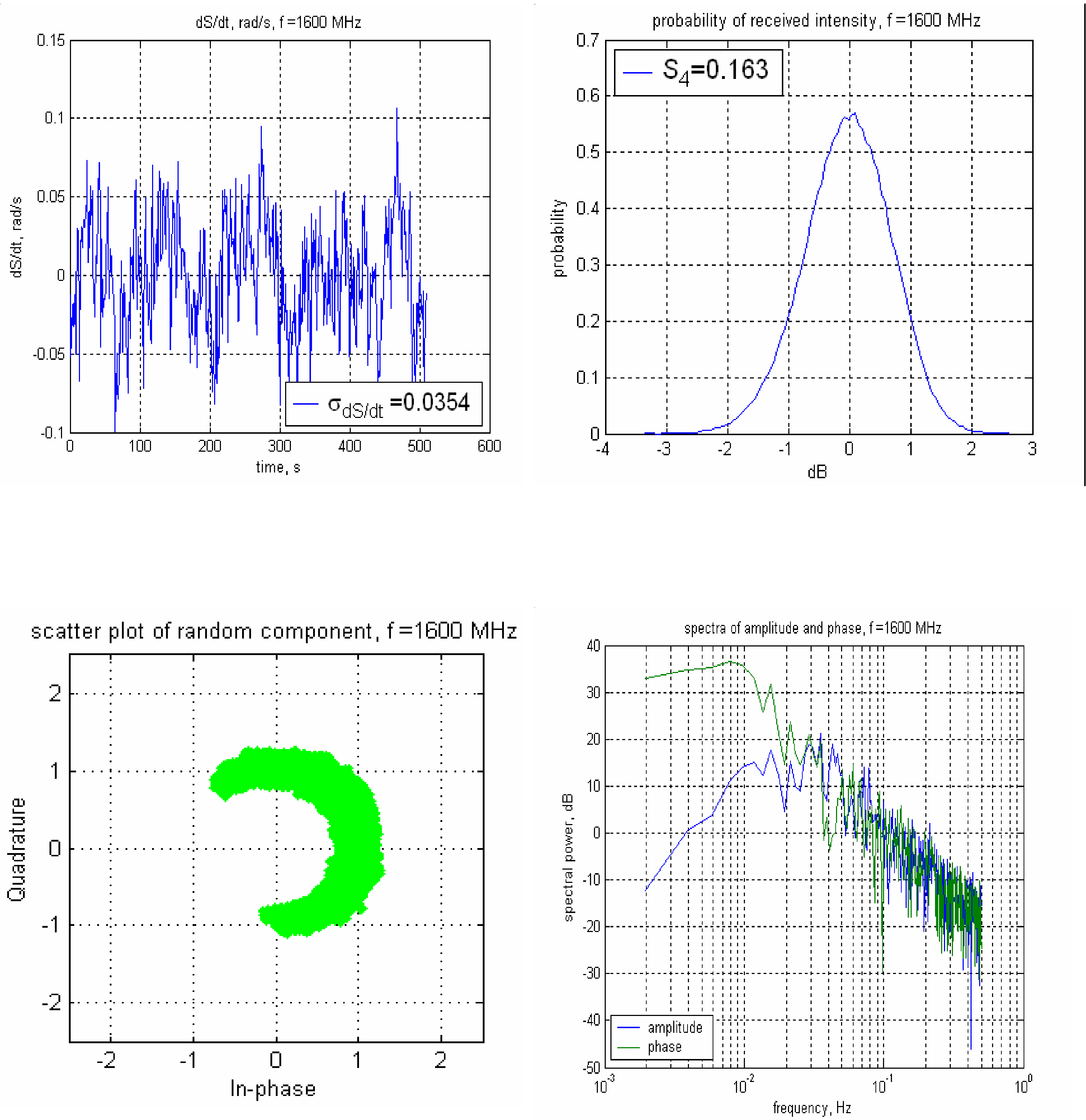

Figure 7b. The intermediate case. Frequency 1600 MHz. Fractional electron density r.m.s. of 20%. Weak scintillation with S_4=0.163 and a symmetric probability density function of the intensity fluctuations. Also shown are the rate of phase change, the phasor R random walk, and the fading frequency spectra of phase and log-amplitude.

Conclusions

The presented technique is capable of producing statistical characteristics and of simulating time realisations of the field (including the regime of strong amplitude fluctuations) for a wide range of the input parameters, viz.:

co-ordinates of the satellite and point of observation slant electron density profile along a given path zenith angle of a satellite magnetic azimuth of the plane of propagation magnetic field dip angle at the pierce point the following parameters of the random irregularities:

- spectral index
- minimal outer scale across the geomagnetic field
- aspect ratios along and across the geomagnetic field
- variance of the fractional electron density fluctuations
- effective velocity of the drift

In the current presentation the technique was employed to determine and discuss the scintillation effects in the polar ionosphere.

References

1. ***V.E.Gherm, N.N.Zernov, and H.J.Strangeways***, «Propagation model for transionospheric fluctuating paths of propagation: Simulator of the transionospheric channel», ***Radio Science***, ***40***, RS1003, doi:10.1029/2004RS003097, 2005.

2. ***V.E.Gherm, N.N.Zernov, S.M.Radicella and H.J.Starngeways***, Propagation model for signal fluctuations on transionospheric radio links, ***Radio Science, 35***, 5, 1221-1232, 2000.

3. ***S.A.Maurits, and B. J. Watkins,*** UAF Eulerian Model of the Polar Ionosphere, in Solar Terrestrial Energy Program (STEP): ***Handbook of Ionospheric Models***, edited by R. W. Schunk, pp. 95-123, Utah State University, 1996.

4. ***A.Kulchitsky, S. A. Maurits, B. J. Watkins, and J. McAllister***, **E** x **B** Drift Simulation in an Eulerian Ionospheric Model Using the TVD Numerical Scheme, ***J. Geophys. Res., 110***, A09310, doi: 10. 1029/2005JA011033, 2005.

5. ***E.D.Tereshchenko, N.Yu.Romanova, and A.V.Koustov***, Orientation of the cross-field anisotropy of small-scale ionospheric irregularities and direction of plasma convection, ***Annal. Geophys., 23***, 1227-1237, 2005.

E-mail addresses:

Nikolay Zernov: zernov@paloma.spbu.ru

Vadim Gherm: gherm@paloma.spbu.ru

Hal Strangeways: H.J.Strangeways@leeds.ac.uk

Sergei Maurits: maurits@arsc.edu